We are IntechOpen, the world's leading publisher of Open Access books
Built by scientists, for scientists

4,800
Open access books available

122,000
International authors and editors

135M
Downloads

154
Countries delivered to

Our authors are among the

TOP 1%
most cited scientists

12.2%
Contributors from top 500 universities

BOOK CITATION INDEX

CLARIVATE ANALYTICS

INDEXED

WEB OF SCIENCE™

Selection of our books indexed in the Book Citation Index
in Web of Science™ Core Collection (BKCI)

Interested in publishing with us?
Contact book.department@intechopen.com

Numbers displayed above are based on latest data collected.
For more information visit www.intechopen.com

Wind Farm Connected to a Distribution Network

Benchagra Mohamed

Abstract

This chapter presents power flow study for distribution network connected to wind farm based on induction generators (IG). It provides an overview of wind energy conversion systems (WECS) and their related technologies. The details of turbine components, system configurations, and control schemes are analyzed. Wind farm–distribution network systems are developed by MATLAB/SIMULINK to perform different tests under various operation conditions. The impact of wind speed fluctuation on power flow, grid voltage dynamic stability, and frequency responses are also investigated. The proposed simulator is applied to a 3 MW wind farm, and then the efficacy of the proposed simulator has been validated.

Keywords: renewable energy, wind farm, power control, distribution network, smart grid, power flow, voltage stability, frequency stability

1. Introduction

According to the updated grid codes, wind farms tend to be considered as power generation plants, which should perform in a similar manner to conventional power-generation plants [1]. When large renewable energy sources are integrated into a distribution network, the dynamics and the operations of the network are affected [2]. Installed wind power capacity has been progressively growing over the last two decades. The increase in wind turbine size implies more power output since the energy captured is a function of the square of the rotor radius [3]. The majority of wind turbines operating in the field are grid-connected, and the power generated is directly uploaded to the grid.

The emergence of the smart grid will pose wind energy developers with a new challenge, such as production during high wind speed; wind turbine should be able to continuously supply the grid, and power factor correction (PFC). For wind power applications, wind turbines were mostly operated with induction generators (IGs) [4]. As a network interface, the use of
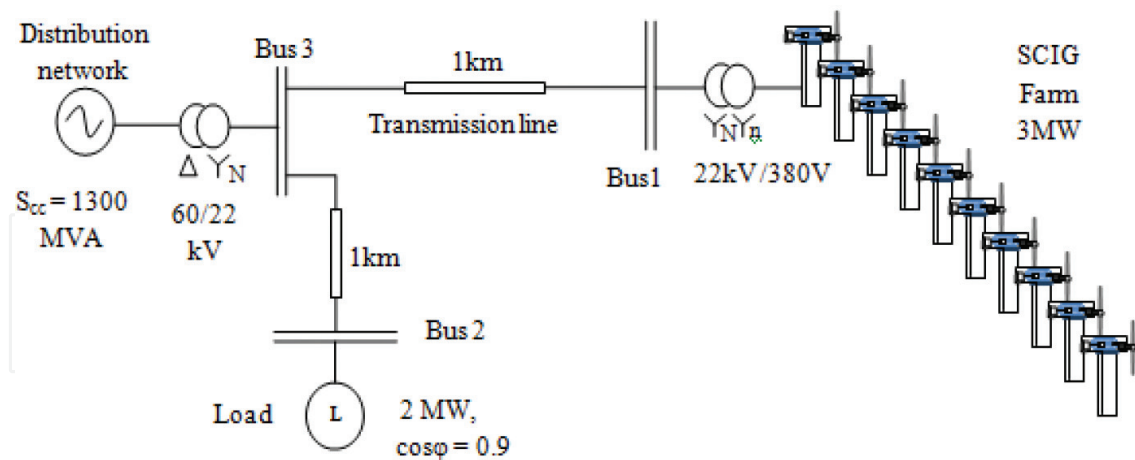
Figure 1. Wind farm–connected distribution network.

converters is extensively reported, showing their capability to extract maximum power in a wide range of wind conditions, and can control both active and reactive powers independently.

The interconnection of wind energy to the power grid is still on the rise. The increasing size of Wind Park resulted in new interconnection grid codes. The power output of wind turbine systems is directly affected by wind speed. Then, when large wind energy sources are integrated into a distribution network as shown in **Figure 1**, the dynamics and the operations of the network are affected [5].

The real and reactive power sharing can be achieved by controlling two independent quantities: the frequency and the voltage magnitude [6]. Any voltage or frequency fluctuation in the wind farm side has direct impact on the grid side [7]. The rotor voltage source converter (VSC) is controlled to maximize the generated power, and the grid VSC is controlled to produce good power quality [8].

The rest of the chapter is organized as follows: in Section 2, the fundamental properties of a WT and its mathematical model are summarized; Section 3 describes the design and control of the Induction Generator and back-to-back converter; Section 4 describes the distribution network connected to wind farm; Section 5 is devoted to the performance simulation of power flow and voltage dynamic stability by MATLAB-SimPowerSystems; and, finally, Section 6 includes the conclusions.

2. Modeling of wind turbine

2.1. Variable-speed wind turbine system configuration

The performance of the wind energy system can be greatly enhanced with the use of a full-capacity power converter. **Figure 2** shows the schematic diagram of the studied wind turbine based on induction generators. All of the subsystem components: WT, VSC, Voltage Source Inverter(VSI), PI controller, transformer, filter, and distribution system, are modeled individually.
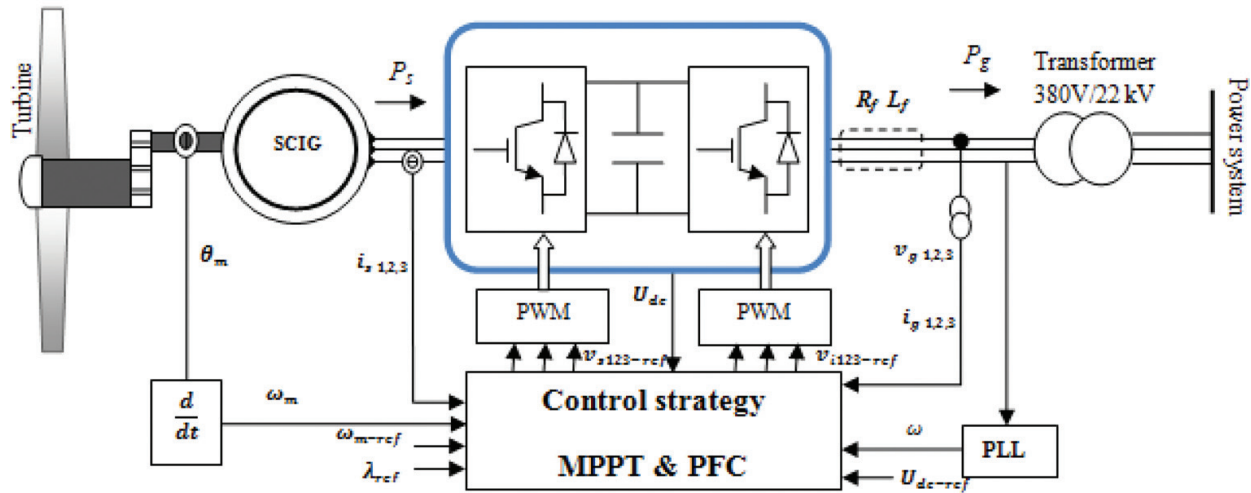
Figure 2. Control of wind turbine.

With the use of the power converter, the generator is fully decoupled from the grid, and can operate in full speed range. This also enables the system to perform reactive power compensation and smooth the grid connection. The turbine rotor shaft of the studied squirrel cage induction generator (SCIG) is coupled to the hub of the turbine through a gearbox for transforming the low rotational speed of the turbine to the required higher rotational speed of the generator. **Figure 3** shows a wind turbine model. The generator converts mechanical energy to electrical energy. The converter is the interface between the generator and the distribution network [4]. The controllers provide proper switching signals for the VSC-SGIC side so as to extract the maximum power from the WT and VSI-grid side to control the voltage and frequency by using a phase-locked loop (PLL) process.
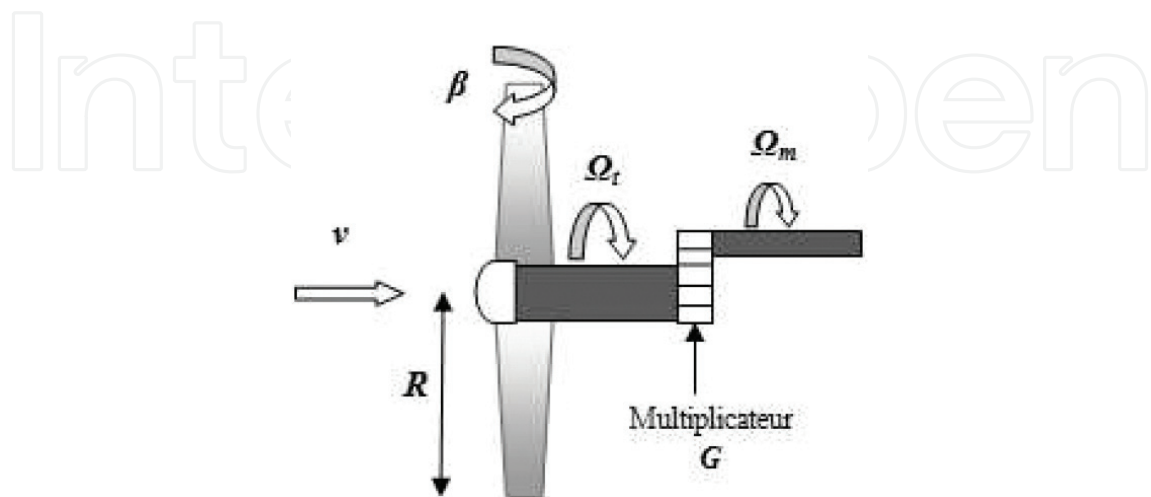

Figure 3. Wind turbine.

2.2. The wind turbine model

A wind energy conversion system (WECS) transforms wind kinetic energy to mechanical energy by using rotor blades. This energy is then transformed into electric energy by a generator, so the turbine is one of the most important elements in wind turbine. In order to better understand the process of wind energy conversion, descriptions of the major parts of a wind turbine are given in this section.

The model of the WT and pitch control is developed on the basis of the steady-state power characteristics of the turbine. The mechanical torque produced by the WT is given by [4]:

$$T_m = \frac{\rho \pi R^2}{\Omega_t} v^3 C_p(\beta, \lambda) \tag{1}$$

where $\rho\ kg/m^3$ is the air density, $R\ m$ is the radius of the turbine, and $v\ m/s$ is the wind velocity. $C_p(\beta, \lambda)$ is the power coefficient that is dependent on the turbine design, Ω_t is the turbine speed, it is a function of mechanical speed ω_m and gear ratio G, $\Omega_t = \frac{\omega_m}{G}$. β is the rotor-blade-pitch angle, and $\lambda = \frac{\Omega_t R}{v}$ is the tip speed ratio [9]. The gearbox conversion ratio, also known as the gear ratio, is designed to match the high-speed generator with the low-speed turbine blades.

As can be observed from Eq. (1), there are three possibilities for increasing the power captured by a wind turbine: the wind speed v, the power coefficient Cp, and the sweep area $A = \pi R^2$.

The power characteristics of a wind turbine are defined by the power curve, which relates the mechanical power of the turbine to the wind speed. It is a highly nonlinear function. The power curve is a wind turbine's certificate of performance that is guaranteed by the manufacturer [1].

The wind turbine input power usually is

$$P_v = \frac{1}{2} \rho A v^3 \tag{2}$$

The output mechanical power of wind turbine is

$$P_m = C_p P_v \tag{3}$$

We consider a generic equation to model the power coefficient C_p, based on the modeling turbine characteristics described in Ref. [10]:

$$C_p(\lambda, \beta) = 0.5109 \left(\frac{116}{\lambda_i} - 0.4\beta - 5 \right) exp \left(\frac{-21}{\gamma} \right)$$
$$\gamma = \left(\frac{1}{(\lambda + 0.08\beta)} - \frac{0.035}{(\beta^3 + 1)} \right)^{-1} \tag{4}$$

where λ is defined as the ratio of the tip speed of the turbine blades to wind speed:

$$\lambda = \frac{R\Omega_t}{v} = \frac{R\omega_m}{Gv} \tag{5}$$

Ω_t is the turbine speed, it is a function of mechanical speed ω_m and gear ratio G [11].

Mechanical equation for the drive train (gearbox) is done by

$$J\frac{d\Omega_m}{dt} = \sum T \tag{6}$$

and

$$\sum T = T_m - T_{em} \tag{7}$$

where T_{em} is the electromagnetic torque, and T_m is the mechanical torque. J is the total inertia, it can be calculated as

$$J = \frac{J_t}{G^2} + J_g \tag{8}$$

where J_t and J_g are respectively, the turbine inertia and the generator inertia.

The power captured by the wind turbine is a cubic function of wind velocity (see Eq. (2)) until the wind speed reaches its rated value. To deliver captured energy to the distribution network at different wind velocities, the induction generator should be properly controlled according to the wind speed in order to extract the maximum power available.

Because of the maximum $C_p(\lambda, \beta)$ is obtained at a optimal tip speed ratio $\lambda = \lambda_{opt}$, looking for taking the maximum power available at any wind speed, the control system must adjust the mechanical speed to operate at λ_{opt}.
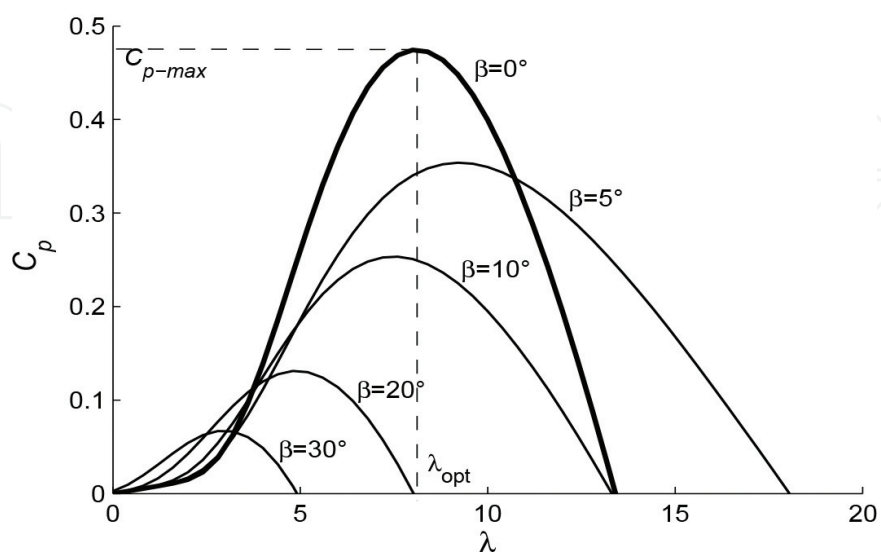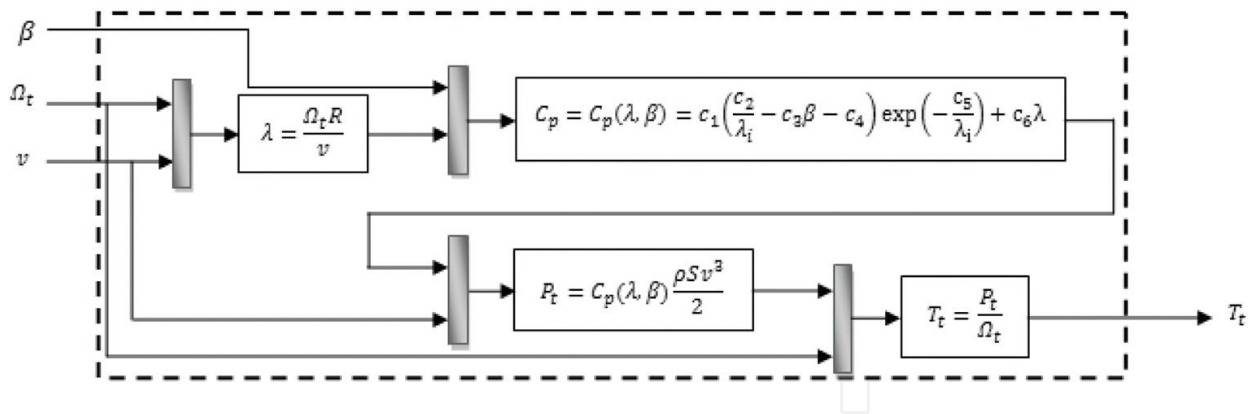

Figure 4. Power coefficient C_p.

Figure 5. Modeling of wind turbine.

A relationship between C_p and γ for various values of the pitch angle β is illustrated in **Figure 4**. The maximum value of C_p, that is $C_{p-max} = 0.47$, is achieved for $\beta = 0$ and for $\lambda_{opt} = 8.1$. The optimal tip speed ratio $\lambda_{opt} = 8.1$ is a constant for a given blade. The equation 4 indicates that in order to obtain the maximum power and conversion efficiency, the turbine speed must be made adjustable according to the wind speed. The model of wind turbine is illustrated in **Figure 5**.

3. Induction generator model

The conversion of mechanical energy to electric energy is performed by the turbine and the generator. Different generator types have been used in wind energy systems. These include the squirrel cage induction generator (SCIG), doubly fed induction generator (DFIG), and synchronous generator (SG) [1].

The SCIG is simple and rugged in construction. It is relatively inexpensive and requires minimum maintenance. The SCIGs are also employed in variable-speed wind energy systems. To date, the largest SCIG wind energy systems are around 4 MW in offshore wind farms.

When the stator winding is connected to a distribution network, a rotating magnetic field is generated in the air gap of this machine. The rotating field induces a three-phase current in the rotor bars, which interacts with the rotating field to produce the electromagnetic torque as shown in **Figure 6**.

The voltage equations for the stator and rotor of the generator in the arbitrary reference frame are given by

$$\frac{d}{dt}\begin{pmatrix} \phi_{sa} \\ \phi_{sb} \\ \phi_{sc} \end{pmatrix} = \begin{pmatrix} v_{sa} \\ v_{sb} \\ v_{sc} \end{pmatrix} - \begin{pmatrix} R_s & 0 & 0 \\ 0 & R_s & 0 \\ 0 & 0 & R_s \end{pmatrix} \cdot \begin{pmatrix} i_{sa} \\ i_{sb} \\ i_{sc} \end{pmatrix} \qquad (9)$$

and

$$\frac{d}{dt}\begin{pmatrix}\phi_{ra}\\\phi_{rb}\\\phi_{rc}\end{pmatrix} = -\begin{pmatrix}R_r & 0 & 0\\0 & R_r & 0\\0 & 0 & R_r\end{pmatrix} \cdot \begin{pmatrix}i_{ra}\\i_{rb}\\i_{rc}\end{pmatrix} \tag{10}$$

where

- $\phi_{sa}Z, \phi_{sb}, \phi_{sc}; \phi_{ra}, \phi_{rb}, \phi_{rc}$: stator and rotor flux-linkage vectors (Wb),

- $v_{sa}Z, v_{sb}, v_{sc}$: stator and rotor voltage vectors (V),

- $i_{sa}Z, i_{sb}, i_{sc}; i_{ra}, i_{rb}, i_{rc}$: stator and rotor current vectors (A),

- R_sZ, R_r stator and rotor winding resistances (Ω).

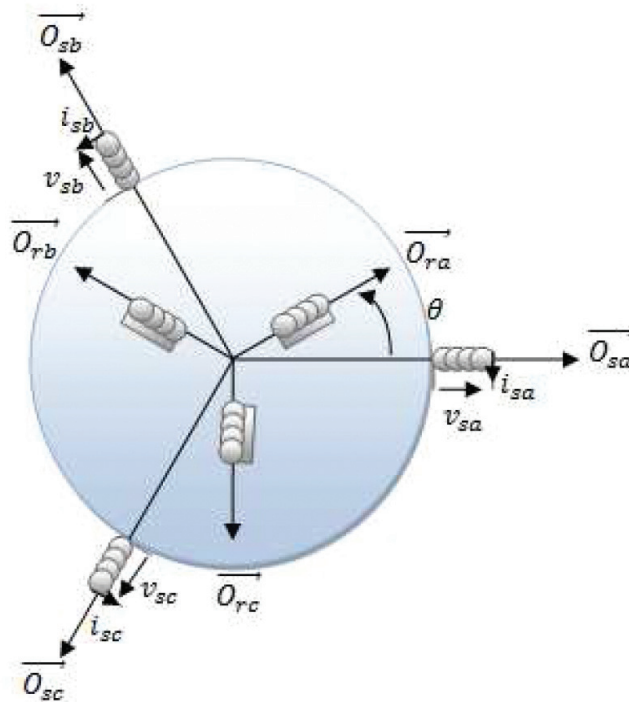**Figure 6.** Representation of IG in electric space.

$$\frac{d}{dt}\left[\phi_{sabc}\right] = [v_{sabc}] - [R_s] \cdot [i_{sabc}] \tag{11}$$

and

$$\frac{d}{dt}\left[\phi_{rabc}\right] = -[R_r] \cdot [i_{rabc}] \tag{12}$$

where

$$[I] = \begin{pmatrix} 1 & 0 & 0 \\ 0 & 1 & 0 \\ 0 & 0 & 1 \end{pmatrix} \tag{13}$$

The second set of equations is for the stator and rotor flux linkages:

$$\begin{pmatrix} \phi_{sabc} \\ \phi_{rabc} \end{pmatrix} = \begin{pmatrix} [L_s] & [M_{sr}] \\ [M_{rs}] & [L_r] \end{pmatrix} \cdot \begin{pmatrix} i_{sabc} \\ i_{rabc} \end{pmatrix} \tag{14}$$

where

$$[L_s] = \begin{pmatrix} l_s & m_s & m_s \\ m_s & l_s & m_s \\ m_s & m_s & l_s \end{pmatrix} \tag{15}$$

where

l_s: self-inductances for stator windings,

m_s: mutual inductances for stator windings.

and

$$[L_r] = \begin{pmatrix} l_r & m_r & m_r \\ m_r & l_r & m_r \\ m_r & m_r & l_r \end{pmatrix} \tag{16}$$

where

l_r: self-inductances for rotor windings,

m_r: mutual inductances for rotor windings

and :

$$[M_{sr}] = M_{max} \begin{pmatrix} \cos(p\theta) & \cos\left(p\theta - \dfrac{2\pi}{3}\right) & \cos\left(p\theta - \dfrac{4\pi}{3}\right) \\ \cos\left(p\theta - \dfrac{4\pi}{3}\right) & \cos(p\theta) & \cos\left(p\theta - \dfrac{2\pi}{3}\right) \\ \cos\left(p\theta - \dfrac{2\pi}{3}\right) & \cos\left(p\theta - \dfrac{4\pi}{3}\right) & \cos(p\theta) \end{pmatrix} \tag{17}$$

The third and final equation is the motion equation, which describes the dynamic behavior of the rotor mechanical speed in terms of mechanical and electromagnetic torque:

$$J\frac{d\omega_m}{dt} = T_e - T_m \tag{18}$$

The third and final equation is the motion equation, which describes the dynamic behavior of the rotor mechanical speed in terms of mechanical and electromagnetic torque.

3.1. Reference frame transformation

The transformation of variables between the three-phase stationary frame (abc frame) and the synchronous frame (dq rotating frame) is presented below.

3.1.1. abc/αβ Reference frame transformation

The transformation of three-phase variables in the stationary reference frame into the two-phase variables also in the stationary frame is often referred to as abc/$\alpha\beta$ transformation. Since the $\alpha\beta$ reference frame does not rotate in space

$$\left[x_{o\alpha\beta}\right] = \left[T_3\right] \cdot \left[x_{abc}\right] \tag{19}$$
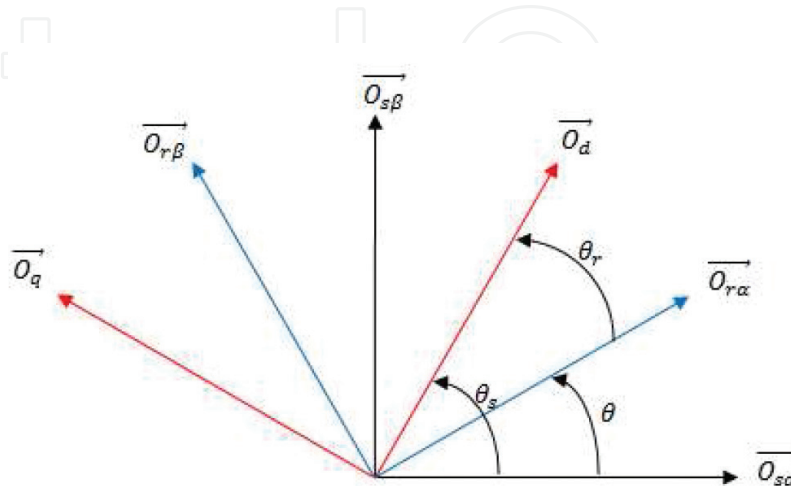
where

$$T_3 = \sqrt{\frac{2}{3}} \begin{pmatrix} \dfrac{1}{\sqrt{2}} & 1 & 0 \\ \dfrac{1}{\sqrt{2}} & \dfrac{-1}{2} & \dfrac{\sqrt{3}}{2} \\ \dfrac{1}{\sqrt{2}} & \dfrac{-1}{2} & \dfrac{\sqrt{-3}}{2} \end{pmatrix} \tag{20}$$

3.1.2. abc/dq Reference frame transformation

To transform variables in the abc stationary frame to the dq rotating frame, simple trigonometric functions can be derived from the orthogonal projection of the a, b, and c variables to the dq-axis as shown in **Figure 7**.

The transformation of the *abc* variables to the *dq* frames, referred to as abc/dq transformation, can be expressed in a matrix form:

Figure 7. Transformation of (abc) stationary frame to the two phase (dq) arbitrary frame.

$$\left[x_{dqo}\right] = \left[P(\psi)\right] \cdot \left[x_{abc}\right] \tag{21}$$

where

$$[P(\psi)] = \sqrt{\frac{2}{3}} \begin{pmatrix} \cos(p\psi) & \cos\left(p\psi - \dfrac{2\pi}{3}\right) & \cos\left(p\psi - \dfrac{4\pi}{3}\right) \\[2mm] \sin(p\psi) & -\sin\left(p\psi - \dfrac{2\pi}{3}\right) & -\sin\left(p\psi - \dfrac{4\pi}{3}\right) \\[2mm] \dfrac{1}{\sqrt{2}} & \dfrac{1}{\sqrt{2}} & \dfrac{1}{\sqrt{2}} \end{pmatrix} \tag{22}$$

where

- $\psi = \theta_s Z$, for stator variables;

- $\psi = \theta_r Z$, for rotor variables.

So Eqs. (12) and (14) can be rewritten as

$$\frac{d}{dt}\left[\phi_{sdqo}\right] = \left[v_{sdqo}\right] - \left[R_s\right] \cdot \left[i_{sdqo}\right] - \left[\Theta\right] \cdot \left[\phi_{sdqo}\right]\frac{d\theta_s}{dt} \tag{23}$$

$$\frac{d}{dt}\left[\phi_{rdqo}\right] = -\left[R_r\right] \cdot \left[i_{rdqo}\right] - \left[\Theta\right] \cdot \left[\phi_{rdqo}\right]\frac{d\theta_r}{dt} \tag{24}$$

where

$$[\Theta] = \begin{pmatrix} 0 & -1 & 0 \\ 1 & 0 & 0 \\ 0 & 0 & 0 \end{pmatrix} \tag{25}$$

the dq rotating frame, the flux, and currents are related by

$$\begin{pmatrix} \phi_{sdqo} \\ \phi_{rdqo} \end{pmatrix} = \begin{pmatrix} [L_{sP}] & [M_{srP}] \\ [M_{rsP}] & [L_{rP}] \end{pmatrix} \cdot \begin{pmatrix} i_{sdqo} \\ i_{rdqo} \end{pmatrix} \tag{26}$$

where

$$[L_{sP}] = \begin{pmatrix} l_s - m_s & 0 & 0 \\ 0 & l_s - m_s & 0 \\ 0 & 0 & l_s - m_s \end{pmatrix} \tag{27}$$

$$[L_{rP}] = \begin{pmatrix} l_r - m_r & 0 & 0 \\ 0 & l_r - m_r & 0 \\ 0 & 0 & l_r - m_r \end{pmatrix} \tag{28}$$

3.2. Back-to-back PWM converter

Power converters are widely used in wind power systems. (In fixed-speed, the converters are used to reduce inrush current during the system start-up, whereas in variable-speed, they are employed to control the speed/torque of the generator and also the active/reactive power to the grid) [1], where a back-to-back converter configuration with two identical PWM converters is used. The converters can be either voltage source converters (VSCs) or current source converters (CSCs)

In wind energy conversion systems, the converter is often connected to an electric grid and delivers the power generated from the generator to the grid. The converter in this application is referred to as a grid-connected or grid tied converter.

4. Control of wind turbine and induction generator

In variable-speed squirrel cage induction generator (SCIG) wind energy conversion systems, full-capacity power converters are required to adjust the speed of the generator in order to harvest the maximum possible power available from the wind. The generator-side converter (rectifier) is used to control the speed or torque of the generator with a maximum power point tracking (MPPT) (see **Figures 8** and **9**). The grid-side converter (inverter) is employed for the control of DC link voltage and grid-side reactive power. The system dynamic and steady-state performance are analyzed. The analysis is assisted by computer simulations and steady-state equivalent circuits.

4.1. MPPT control

The main goal of control is to maximize the wind power capture at different wind speeds, which can be achieved by adjusting the turbine speed in such a way that the optimal tip speed ratio $\lambda_{opt}t$ is maintained.
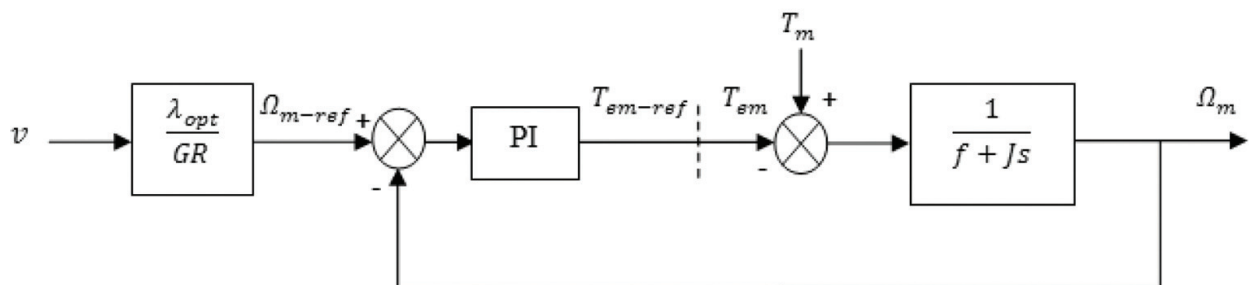
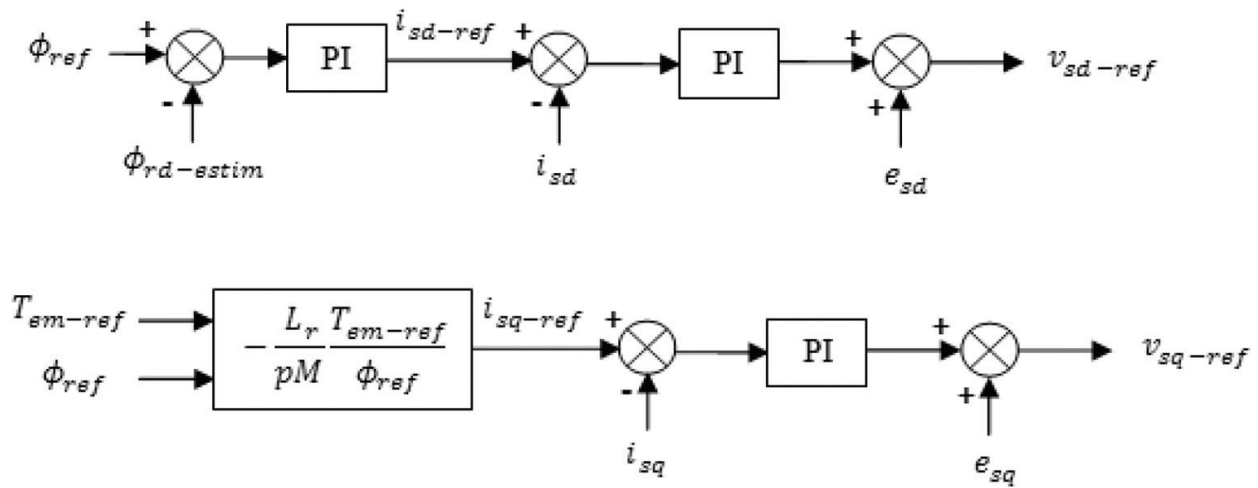**Figure 8.** Control of mechanical speed Ω_m.
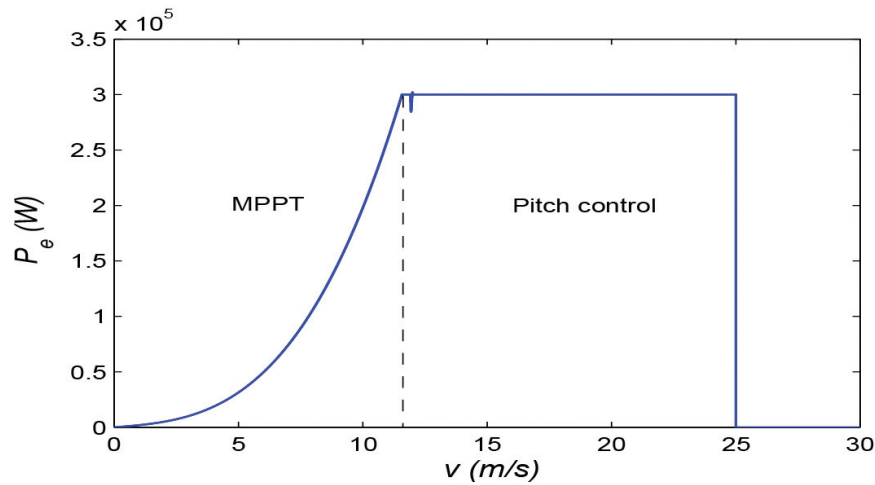
Figure 9. Vector control of SCIG.

Figure 10. Wind turbine characteristic.

Control laws developed in this chapter are validated by simulations of the global wind behavior, applying a profile variable wind that can test these laws under and above the rated wind speed. This command allows to operate the wind so as to extract the maximum power of energy (MPPT) when the wind speed is below its nominal value and the limit above this speed (pitch control) as shown in **Figure 10**, and finally injecting a sinusoidal current in phase with the line voltage (PFC).

We note that the increase of β allows to degrade C_p coefficient and therefore causes the decrease in the mechanical power recovered on the axis of the wind turbine, simulation results are shown in **Figures 11**, **12** and **13**.
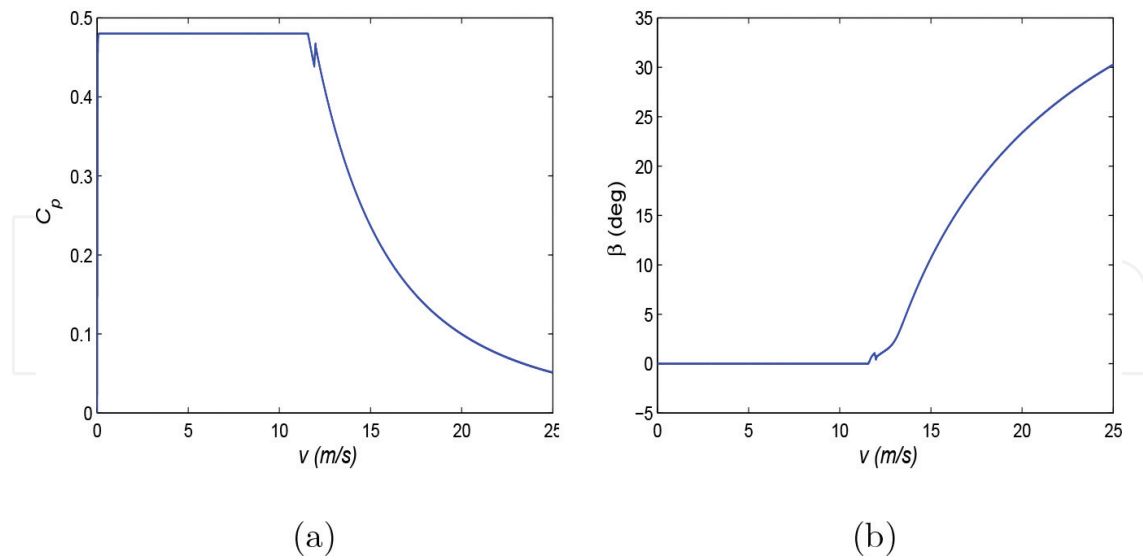
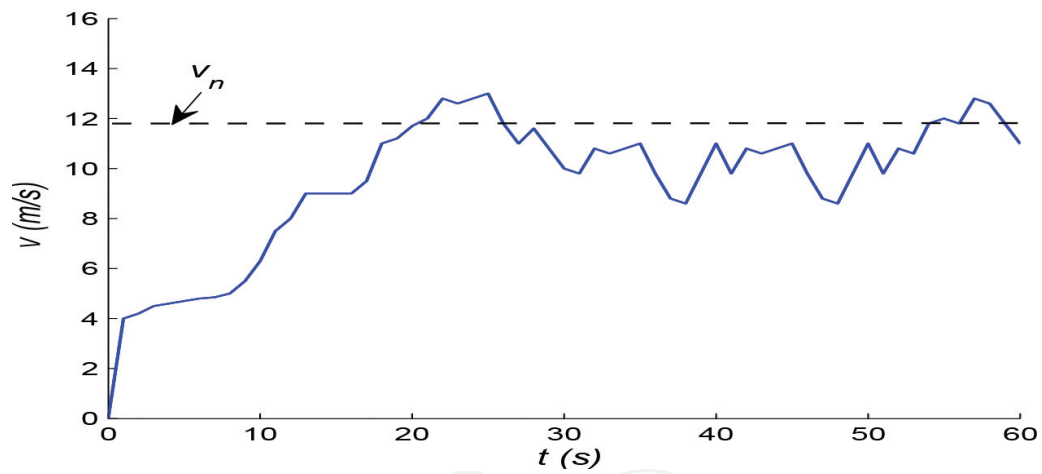**Figure 11.** Variation of aerodynamic variables: (a) power coefficient C_p; (b) pitch angle β.
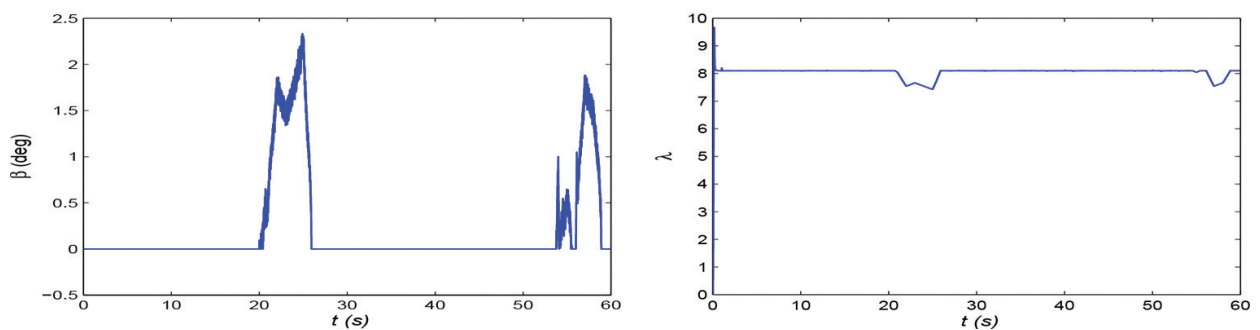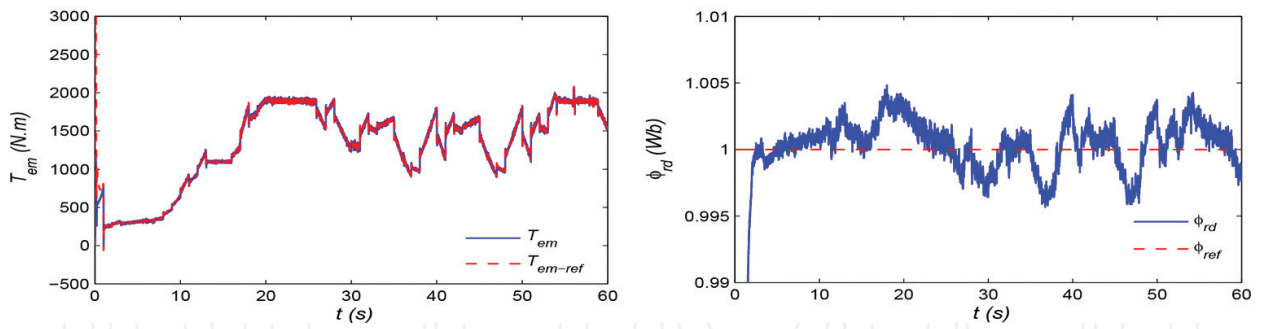

Figure 12. Wind velocity profile.

Figure 13. Impact on aerodynamic variables: (a) Pitch angle; (b) speed ratio β; speed ratio λ.

Figure 14. Variation of electromagnetic variables: (a) Electromagnetic torque; (b) Rotor flux.

Figure 14 presents the variation of electromagnetic torque and the rotor flux, as desired, they are tracked to their input references.

5. Control of grid-connected converter

A typical grid-connected inverter for wind energy applications is shown in **Figure 2**. The inverter is connected to the grid through a line inductance L_f, which represents the leakage inductance of the transformer. The power flow between the converter and the grid is bidirectional. Power can be transferred from the DC circuit of the converter to the grid. The grid power factor can be unity. It is often required by the grid operator that a wind energy system provide a controllable reactive power to the grid to support the grid voltage in addition to the active power production.

The grid-connected converter can be controlled with voltage-oriented control, as shown in **Figure 2**. According to **Figure 2**, the relationship between the grid, converter voltages, and line currents is given as follows:

$$\begin{pmatrix} v_{i1} \\ v_{i2} \\ v_{i3} \end{pmatrix} = R_f \begin{pmatrix} i_{g1} \\ i_{g2} \\ i_{g3} \end{pmatrix} + L_f \frac{d}{dt} \begin{pmatrix} i_{g1} \\ i_{g2} \\ i_{g3} \end{pmatrix} + \begin{pmatrix} v_{g1} \\ v_{g2} \\ v_{g3} \end{pmatrix} \tag{29}$$

Transforming the voltage Eq. (29) using dq transformation in the rotating reference frame at the grid frequency gives

$$\begin{pmatrix} v_{id} \\ v_{iq} \end{pmatrix} = R_f \begin{pmatrix} i_{gd} \\ i_{gq} \end{pmatrix} + L_f \frac{d}{dt} \begin{pmatrix} i_{gd} \\ i_{gq} \end{pmatrix} \begin{pmatrix} i_{gd} \\ i_{gq} \end{pmatrix} + L_f \omega_g \frac{d}{dt} \begin{pmatrix} -i_{gq} \\ i_{gd} \end{pmatrix} + \begin{pmatrix} v_{gd} \\ v_{gq} \end{pmatrix} \tag{30}$$

where ω_g is the speed of the synchronous reference frame. This indicates that the system control is cross-coupled, which may lead to difficulties in controller design and unsatisfactory

dynamic performance. To solve the problem, a decoupled controller can be implemented. We consider the following couplings voltages:

$$\begin{pmatrix} e_d \\ e_q \end{pmatrix} = L_f \omega_g \frac{d}{dt} \begin{pmatrix} -i_{gq} \\ i_{gd} \end{pmatrix} \tag{31}$$

$$\begin{pmatrix} \Delta v_{fd} \\ \Delta v_{fq} \end{pmatrix} = R_f \begin{pmatrix} i_{gd} \\ i_{gq} \end{pmatrix} + L_f \frac{d}{dt} \begin{pmatrix} i_{gd} \\ i_{gq} \end{pmatrix} \tag{32}$$

The decoupled control makes the design of the PI controllers more convenient, and the system is more easily stabilized.

The equation for the voltage across the DC-bus is given by

$$C \frac{dU_{dc}}{dt} = i_s - i_g \tag{33}$$

This yields to

$$CU_{dc} \frac{dU_{dc}}{dt} = U_{dc} i_s - U_{dc} i_g \tag{34}$$

Eq. (34) can be rewritten as

$$CU_{dc} \frac{dU_{dc}}{dt} = P_s - P_g \tag{35}$$

From Eq. (35), the DC-bus voltage controller provides the active power reference value (or direct grid current reference) and Ps acts as a disturbance. The equation 34 can be presented as differential equations for DC-bus voltage and the grid currents [11].

To realize this control, the grid voltage is measured and its angle is detected for the voltage orientation. This angle is used for the transformation of variables from the abc stationary frame to the dq synchronous frame through the abc/dq transformation.

$$P_g = \frac{3}{2} \left(v_{dg} i_{dg} - v_{qg} i_{qg} \right) \tag{36}$$

$$Q_g = \frac{3}{2} \left(v_{qg} i_{dg} - v_{dg} i_{qg} \right) \tag{37}$$

To achieve the control scheme, the d-axis of the synchronous frame is aligned with the grid voltage vector; therefore, the d-axis grid voltage is equal to its magnitude ($v_{qd} = v_g$) and the resultant q-axis voltage v_{gq} is then equal to zero ($v_{gq} = 0$), from which the active and reactive power of the system can be calculated.

The initial angle of the phase 1 is set to 0 and, the initial angle of the d–q reference frame is set to $\frac{\pi}{2}$, and this causes the v_{gq} component to be zero and the v_{gd} component to be equal to simple phase voltage v_{g1}.

In this reference frame, the above P and Q equations will become [11]

$$P_g = \frac{3}{2} v_{dg} i_{dg} \tag{38}$$

$$Q_g = -\frac{3}{2} v_{dg} i_{qg} \tag{39}$$

Thus the active and reactive power flows are controlled by the i_{gd} and i_{gd}, respectively

5.1. Dynamic and steady-state analysis

The application of wind turbine power quality characteristics to determine the impact of wind turbines on voltage quality is explained through a case study considering a 3 MW wind farm on a 22 kV distribution network. To study the operation and performance of the SCIG wind energy system, some case studies are provided. One investigates the power dynamic behavior of the system, the impact on voltage and frequency, and another analyses the power quality performance of the system with a change in wind speeds. The control architecture of this conversion chain consists of different control blocks (see **Figure 15**).

5.2. Active and reactive power flow

The reactive power exchange with the grid is determined by the voltage and current of the grid side of the power electronic converter. In this case, the wind turbine is fully decoupled from the
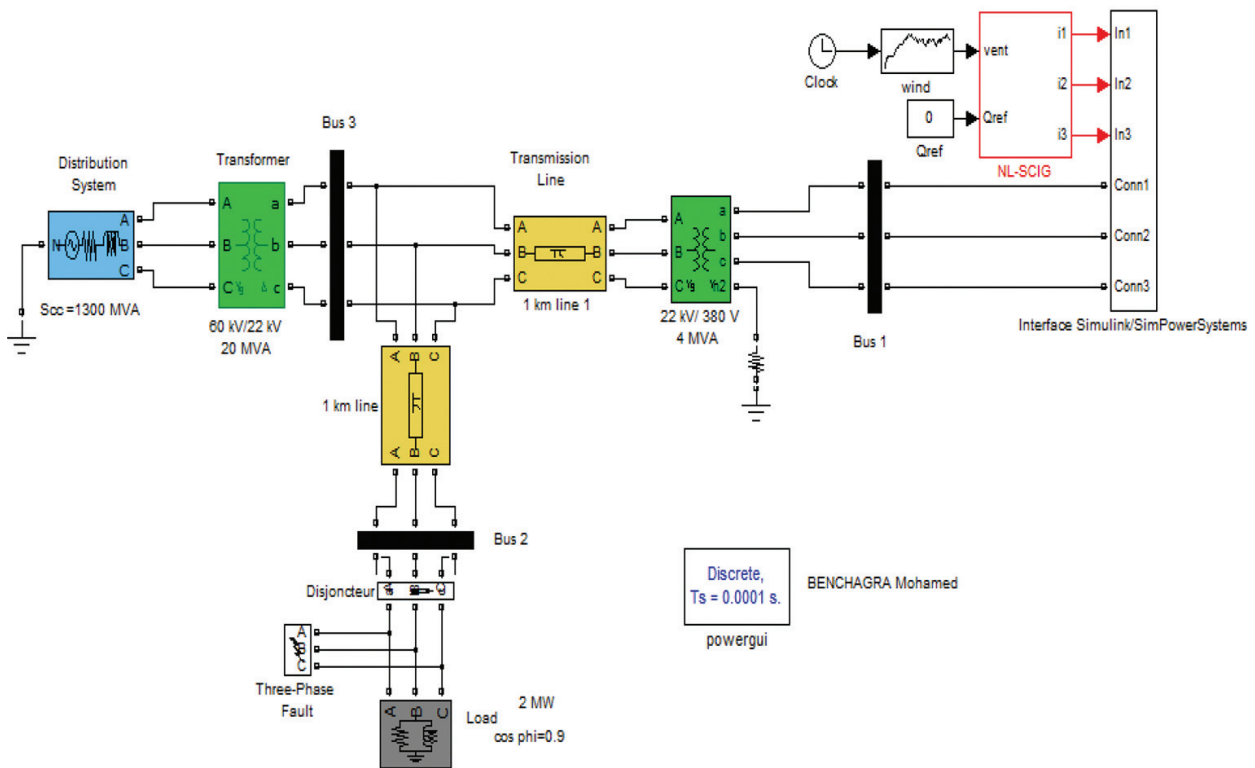
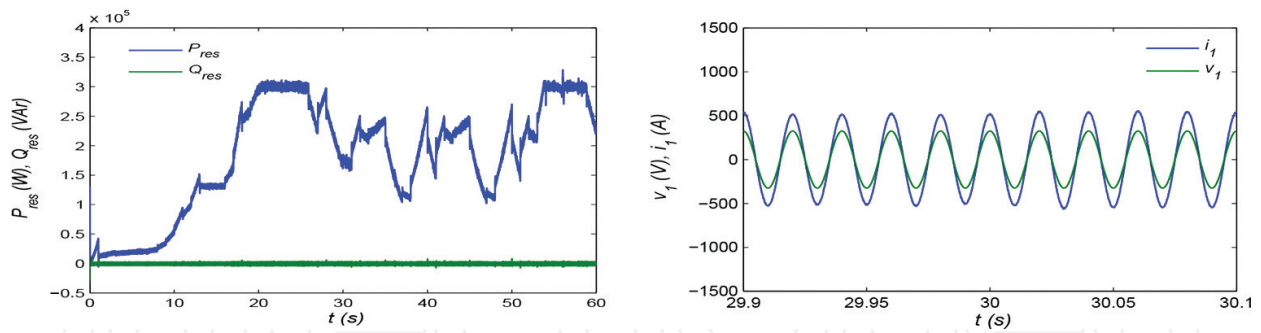**Figure 15.** Simulation model of wind farm–connected distribution network.

Figure 16. Variation of electric variables: (a) Active and reactive power; (b) voltage and current of wind turbine.
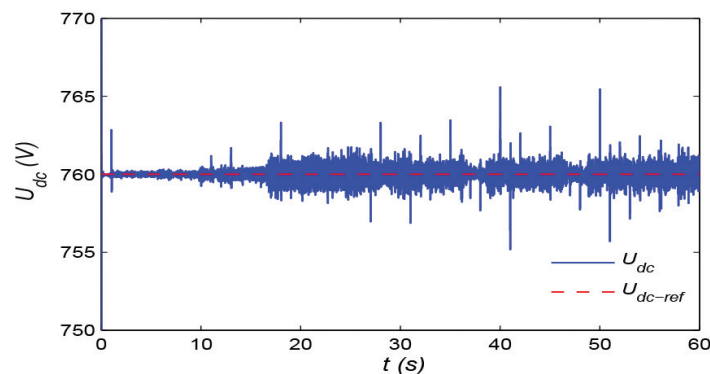

Figure 17. DC bus voltage.

grid. This means that the power factor of the wind turbine and the power factor of the power network side can be controlled independently. **Figure 16** shows the response of the system for a variable wind velocity. During test, the active and reactive powers are decoupled. **Figure 17** shows the DC-bus voltage of the back-to-back converter, as desired, the voltage is kept at their reference value.

5.3. Impact on voltage and frequency

The principal function of power network system is to transport and distribute electrical power from the generators to the loads. In order to function normally, it is essential that the voltage is kept close to its nominal value, so it is becoming increasingly important, for wind farm connected to the transmission system and for those connected to the distribution system, to be able to contribute to voltage control [12, 13]. This section looks at the impact of wind power on voltage control. However, even though there is a voltage difference between the two ends of the branch, the node voltage is not allowed to deviate from the nominal value of the voltage in excess of a certain value (normally 5% to 10%).

Ideally, the voltage should form a perfect sinusoidal curve with constant frequency and amplitude. However, in any real-life power system, grid-connected appliances will cause the voltage to deviate from the ideal [14] (**Figure 18 (a)**).
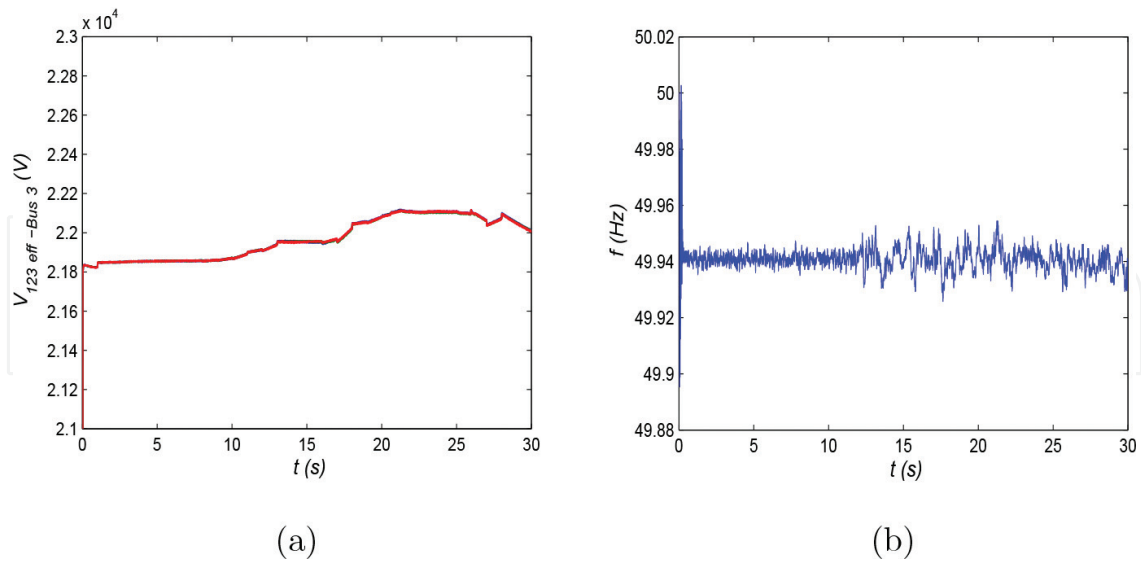
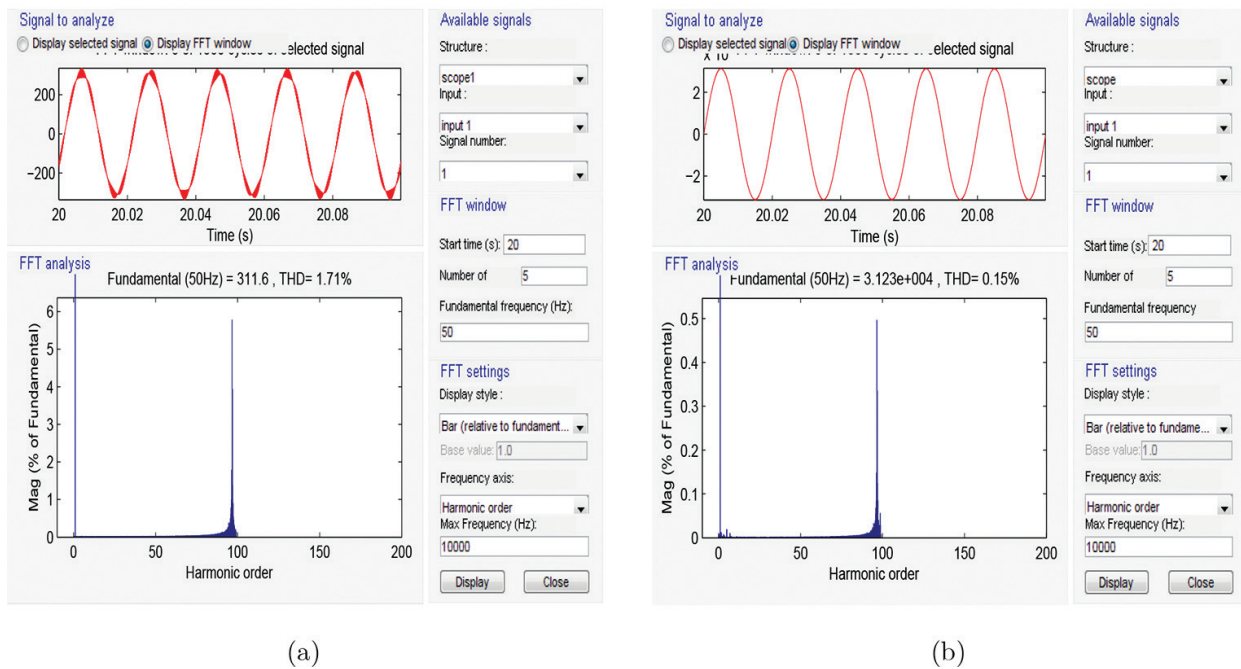**Figure 18.** Impact on Bus 3: (a) voltage; (b) frequency.

Figure 19. Harmonic analysis: (a) On Busbar 1; (b) On Busbar 3.

As can be seen, the adopted control strategy is capable of providing accurate tracking of voltage and frequency at normally values.

5.4. Power quality – harmonics

The application of power quality characteristics defined in IEC 61400–21 to determine the impact of wind turbines on voltage quality is explained in our case study by considering a

3 MW wind farm on a 22 kV distribution network. Certainly, if the wind farm is large or the grid is very weak, additional analyses may be required to assess the impact on power system stability and operation.

Nonlinear loads distort the voltage waveform and may in severe cases cause an overheating of neutral conductors and electrical distribution transformers.

The emission of harmonic currents and voltages of a wind farm with a back-to-back converter has to be stated. **Figure 19** illustrates the harmonic analysis on Busbar 1 and Busbar 3 of the proposed model. Its spectral analysis brings up by presence of the switching frequency (5 kHz) and a distortion (THD = 0.15%) of the effective value of the fundamental component of the voltage in Busbar 3 (Point of Common coupling). The results clearly show that the spread of harmonic current generated by wind turbines fit into the user standards.

6. Conclusion

This chapter discussed the impact of wind farm on the dynamics of distribution network. After modeling the system and developing the controllers, the obtained results are interesting for wind farm application to ensure better quality of power and to study the effect on power system dynamics or stability while increasing the wind power penetration.

Author details

Benchagra Mohamed

Address all correspondence to: mohamed.benchagra@uhp.ac.ma

University Hassan, ENSA, Khouribga, Morocco

References

[1] B. Wu, Power Conversion and Control of Wind Energy Systems, August 2011, Wiley-IEEE Press, ISBN: 978-0-470-59365-3.

[2] C. Chompoo Inwai, W.J. Lee, P. Fuangfoo, M. Williams, J.R. Liao, System impact study for the interconnection of wind generation and utility system, IEEE Transaction on Industry Applications, 41, 163–168, 2005.

[3] E. Hau, Wind Turbines: Fundamentals, Technologies, Application, Economics, 2nd ed., Springer Berlin Heidelberg, 2005, ISBN 978-3-540-29284.

[4] M. Benchagra, M. Maaroufi, M. Ouassaid, A performance comparison of linear and nonlinear control of a SCIG-wind farm connecting to a distribution network control, Turkish Journal of Electrical Engineering and Computer Sciences 22, 1–11, 2014.

[5] T. Burton, Wind Energy Handbook, John Wiley & Sons Ltd, 2011. ISBN: 978-0-470-69975-1.

[6] F. Blaabjerg, Z. Chen, Power Electronics for Modern Wind Turbines, Morgan & Claypool Publishers, 2006 doi:10.2200/S00014ED1V01Y200602PEL001.

[7] P.M. Pardalos, Handbook of Wind Power Systems, Springer, 2013. ISBN 978-3-642-41080-2.

[8] A. Baggini, Handbook of Power Quality, John Wiley & Sons Ltd, 2008 ISBN: 978-0-470-06561-7.

[9] M. Benchagra, M. Maaroufi, Control of wind farm connected distribution network, 10th IEEE International Conference on Networking Sensing and Control (ICNSC), 2013 10 -12 Apr 2013 , Evry, France.

[10] R. Penta, J.C. Clare, G.M. Asher, Doubly fed induction generator using back-to-back PWM converters and its application to variable speed wind-energy generation, IEE Proceedings – Electric Power Applications, 231–241, 143(3), 1996.

[11] M. Benchagra, Y. Errami, M. Hilal, M. Maaroufi, M. Cherkaoui, M. Ouassaid, New control strategy for inductin generator-wind turbine connected grid, 2012 International Conference on Multimedia Computing and Systems, 2012;10–12 May 2012, Tangiers, Morocco.

[12] D. Devaraj, R. Jeevajyothi, Impact of fixed and variable speed wind turbine systems on power system voltage stability enhancement. IET Conference on Renewable Power Generation (RPG 2011), 6–8 September 2011 - Edinburgh, UK.

[13] J.G. Slootweg, Wind Power and Voltage Control, Wind Power in Power Systems, 2005 John Wiley & Sons, Ltd , DOI: 10.1002/0470012684.

[14] J.O. Tande, Power Quality Standards for Wind Turbines, Wind Power in Power Systems, T. Ackermann editor, Wind Power in Power Systems, 2012 Second Edition, John Wiley & Sons, Lt, DOI: 10.1002/9781119941842.ch8.